Compressed nuclei in relativistic Thomas-Fermi approximation

T. v. Chossy, P. Marshall, and W. Stocker
Sektion Physik, University of Munich, D-85745 Garching, Germany
(Received 1 April 1999; published 26 October 1999)

We approach the gross structure of compressed nuclei by scaling ground-state relativistic Thomas-Fermi (RTF) densities as well as by performing RTF calculations with a density-dependent constraint as the equivalent for an external pressure. For the NL1 parametrization of the nuclear effective Lagrangian the line of β stability as well as the proton drip lines are found to be bended to neutron-richer nuclei with increasing compression. In addition we conclude from calculated critical $(Z^2/A)_{\mathrm{crit}}$ values that fission barriers are appreciably reduced by the presence of an external pressure. [S0556-2813(99)04311-3]

PACS number(s): 21.60.−n, 21.10.Dr, 21.65.+f, 24.75.+i

I. INTRODUCTION

Direct information on nuclear compressional properties near the ground state can be gained from small-amplitude monopole density vibrations of nuclei. This dynamical mode requires an analysis using the microscopic random-phase approximation in order to extract a reliable value for the static nuclear compression modulus K_∞ (see Ref. [1] and references quoted therein). On this basis recent precision data on the nuclear breathing mode led Youngblood *et al.* [2] to an estimate of the nuclear matter incompressibility K_∞ of 231 ± 5 MeV.

From the intuitive picture of surface tension compressing the interior of a finite nucleus even ground-state properties of nuclei are influenced by the nuclear matter incompressibility. Fits of effective interactions in Hartree-Fock (HF) or Thomas-Fermi (TF) calculations, and of effective relativistic mean-field (RMF) Lagrangians to mainly masses do, however, lead to incompressibilities different by a factor of 2. This might come from the fact that energies, being stationary, are not sensitive to changes of the ground-state densities.

In a recent detailed study Patyk *et al.* [3] compared the quality of the description of masses and radii in various approaches, such as the HF approach, the TF plus Strutinsky integral method [4], the RMF (see, e.g., [5]) and the macroscopic-microscopic approaches [6]. What can be inferred from Ref. [3] is that—independent of whether the approach is nonrelativistic or relativistic—mass fits can be made good on a high level, depending mostly on the expenditure of the fits. However, then there remain deviations of the charge radii from experiment. From Table V in Ref. [3] they seem to be less the more the incompressibilities resemble the value that was extracted in Ref. [2] from breathing mode energies.

Furthermore, it was shown in Refs. [7] and [8] using TF and relativistic Hartree approaches, respectively, that specific surface properties play a key role in order to come to an unambiguous value of K_∞ which was found close to the value of Ref. [2].

Thus, a value for K_∞ has been reached now that follows uniquely from different nuclear properties and methods. In particular it is independent of the theoretical analysis: nonrelativistic as well as relativistic mean-field approaches converge to the same value. This might to some degree be a simple consequence of the fact that both procedures have still some phenomenological aspects leading to an assimilation of the final numerical results.

The present investigation aims at the treatment of the problem of the structure of nuclei which are compressed more than in small-amplitude breathing modes. Nuclei in high-energy heavy-ion reactions are expected to be compressed up to several times the saturation density. Also for astrophysics the structure of compressed nuclei is of interest since highly compressed nuclei might occur in supernova explosions and in neutron stars [9].

The theoretical analysis of heavy-ion collisions uses kinetic equations (see, e.g., Refs. [10]). The equation of state relating nuclear pressure, density, and temperature enters implicitly as the nuclear structure input. Large compressions can no more be represented by K_∞ alone. Moreover, mesonic degrees, and eventually also quark-gluon aspects emerge in such a way that the standard nonrelativistic descriptions with nuclear potentials might not be sufficient.

As a basis for our approach we use the RTF approximation of the σ-ω-ρ model [5] with meson fields explicitly mediating nucleon-nucleon interactions. This method implies a tolerable numerical amount describing, however, only gross structure of nuclei. The NL1 parametrization [11] of the nuclear Lagrangian with its good representation of compression properties around saturation seems to be a good starting point although it overestimates neutron-proton asymmetry effects.

In a rigorous formalism the external pressure has to be simulated by a constraint depending on nuclear densities in order to reflect the experimental conditions. In Refs. [12] the surface structure of compressed semi-infinite nuclear matter (SINM) was studied starting from schematic energy densities as well as from a class of constraints equivalent to external pressures. Systematic calculations of finite nuclei on the basis of constraints might become rather tedious. Therefore, we first point out that the standard compression by scaling the density can be represented by a special constraint, and then concentrate some of our subsequent exploratory considerations using this scaling mode. For a class of bulk compressions proper mass tables are calculated. Then, for a given nuclear compression, the line of β stability can be extracted from the calculated nuclei. Also the proton and neutron drip lines can be obtained. We found a tendency of the proton

drip lines to be shifted in the (N,Z) plane to neutron richer nuclei when pressure is exerted on nuclei. Thus, stable nuclei are expected to become first β^+ unstable under compression, and beyond a critical compression a nucleus will eventually decay under proton emission.

In addition, the critical ratio $(Z^2/A)_{\rm crit}$ for the onset of fission instability is calculated as a function of compression for several representative modes including the scaling mode. One expects from the reduction of the stabilizing surface tension and the increase of the Coulomb energy with compression that nuclei, stable in the ground state, might fission under compression, which from intuition seems somewhat paradox.

II. THE RELATIVISTIC THOMAS-FERMI APPROXIMATION (RTF)

A. Nuclear ground state

The RTF treatment of the ground state of finite nuclei on the basis of the σ-ω-ρ model is well established, see, e.g., [14,5]. Its basic ingredients will be discussed shortly in order to introduce notations and to have a basis to be referred to when the method is generalized for the description of compressed nuclei in the next subsection.

We start from the standard mean-field Lagrangian for the nonlinear σ-ω-ρ model [5]:

$$\mathcal{L}_{\rm MFT}=\overline{\psi}\Big[i\gamma_\mu\partial^\mu-g_{\rm v}\gamma^0V_0-g_\rho\gamma^0\tau_3b_{00}-e\frac{(1+\tau_3)}{2}A_0-(M-g_{\rm s}\phi_0)\Big]\psi-\frac{1}{2}[(\nabla\phi_0)^2+m_{\rm s}^2\phi_0^2]-\frac{1}{3}b\phi_0^3-\frac{1}{4}c\phi_0^4+\frac{1}{2}[(\nabla V_0)^2+m_{\rm v}^2V_0^2]+\frac{1}{2}[(\nabla b_{00})^2+m_\rho^2b_{00}^2]+\frac{1}{2}(\nabla A_0)^2. \quad (1)$$

Besides the meson fields ϕ_0, V_0, and b_{00}, the photon field A_0 and its coupling to the proton current is taken into account.

The RTF densities $\rho_{\rm n}$, $\rho_{\rm p}$, and $\rho_{\rm s}$ are given in terms of the Fermi momenta of neutrons and protons, $k_{\rm F_n}$ and $k_{\rm F_p}$, respectively, by

$$\rho(r)=\rho_{\rm p}(r)+\rho_{\rm n}(r)=\frac{1}{3\pi^2}[k_{\rm F_p}^3(r)+k_{\rm F_n}^3(r)], \quad (2)$$

$$\rho_3(r)=\rho_{\rm p}(r)-\rho_{\rm n}(r)=\frac{1}{3\pi^2}[k_{\rm F_p}^3(r)-k_{\rm F_n}^3(r)], \quad (3)$$

$$\rho_{\rm s}(r)=\frac{2}{(2\pi)^3}\sum_{a={\rm p,n}}\int_{k<k_{{\rm F}_a}(r)}\frac{M^\star(r)}{\epsilon^\star(k,r)}d^3k, \quad (4)$$

$$M^\star(r)=M-g_{\rm s}\phi_0(r), \quad (5)$$

$$\epsilon^\star(k,r)=\sqrt{k^2+M^{\star^2}(r)}. \quad (6)$$

From there the RTF energy density can be written as

$$\mathcal{E}_{\rm RTF}(r)=g_{\rm v}V_0(r)\rho(r)+g_\rho b_{00}(r)\rho_3(r)+eA_0(r)\rho_{\rm p}(r)+\frac{2}{(2\pi)^3}\sum_{a={\rm p,n}}\int_{k<k_{{\rm F}_a}(r)}\epsilon^\star(k,r)d^3k-\frac{1}{2}[V_0'^2(r)+m_{\rm v}^2V_0^2(r)]-\frac{1}{2}[b_{00}'^2(r)+m_\rho^2b_{00}^2(r)]-\frac{1}{2}A_0'^2(r)+\frac{1}{2}[\phi_0'^2(r)+m_{\rm s}^2\phi_0^2(r)]+\frac{1}{3}b\phi_0^3(r)+\frac{1}{4}c\phi_0^4(r). \quad (7)$$

The specific RTF equations for a given nucleus with Z protons, N neutrons, and $A=N+Z$ nucleons are obtained from the minimization of the energy taking care of fixed neutron and proton numbers by introducing Lagrange multipliers $\mu_{\rm n}$ and $\mu_{\rm p}$ as the respective chemical potentials:

$$\delta\left(4\pi\int_0^\infty[\mathcal{E}_{\rm RTF}(r)-\mu_{\rm n}\rho_{\rm n}(r)-\mu_{\rm p}\rho_{\rm p}(r)]r^2dr\right)=0. \quad (8)$$

The RTF equations are given by

$$\left(\frac{d^2}{dr^2}+\frac{2}{r}\frac{d}{dr}-m_{\rm s}^2\right)\phi_0(r)=-g_{\rm s}\rho_{\rm s}(r)+b\phi_0^2(r)+c\phi_0^3(r), \quad (9)$$

$$\left(\frac{d^2}{dr^2}+\frac{2}{r}\frac{d}{dr}-m_{\rm v}^2\right)V_0(r)=-g_{\rm v}\rho(r), \quad (10)$$

$$\left(\frac{d^2}{dr^2}+\frac{2}{r}\frac{d}{dr}-m_\rho^2\right)b_{00}(r)=-g_\rho\rho_3(r), \quad (11)$$

$$\left(\frac{d^2}{dr^2}+\frac{2}{r}\frac{d}{dr}\right)A_0(r)=-e\rho_{\rm p}(r), \quad (12)$$

$$g_{\rm v}V_0(r)+g_\rho b_{00}(r)+eA_0(r)+\epsilon_{\rm F_p}^\star(r)=\mu_{\rm p}\quad(r\leqslant r_{\rm p_u}), \quad (13)$$

$$g_{\rm v}V_0(r)-g_\rho b_{00}(r)+\epsilon_{\rm F_n}^\star(r)=\mu_{\rm n}\quad(r\leqslant r_{\rm n_u}), \quad (14)$$

$$\epsilon_{F_{\rm n,p}}^\star(r)\equiv\sqrt{k_{F_{\rm n,p}}^2(r)+M^{\star^2}(r)}. \quad (15)$$

This set of coupled differential and algebraic equations has to be solved by an iterative procedure in a self-consistent way. The rigorous inclusion of the Coulomb field leads to specific numerical problems which we have overcome by computing a preliminary solution using Fourier-sine series for the meson fields as well as for the Coulomb potential. The classical turning points $r_{\rm n_u}$ and $r_{\rm p_u}$ are characterized by

TABLE I. RTF and RH values of binding energies E_b (MeV) and charge radii r_c (fm) of finite nuclei, calculated for several effective Lagrangians. All values were obtained by calculations without center-of-mass correction and without pairing.

		RTF			RH	
	NL-Z	NL1	NL-SH	NL-Z	NL1	NL-SH
^{40}Ca	E_b=332.3	327.2	324.4	336.4	333.5	331.5
	r_c=3.55	3.54	3.44	3.50	3.50	3.45
^{90}Zr	E_b=775.8	770.0	765.4	778.4	777.9	775.1
	r_c=4.41	4.39	4.30	4.27	4.26	4.24
^{208}Pb	E_b=1619.5	1610.5	1609.6	1631.9	1634.2	1636.9
	r_c=5.73	5.68	5.59	5.56	5.51	5.49

$$\rho_n(r)=0 \quad (r\geqslant r_{n_u}), \quad \rho_p(r)=0 \quad (r\geqslant r_{p_u}). \tag{16}$$

The results following from this RTF approach and the more sophisticated relativistic Hartree (RH) method [5] display characteristic differences. In Table I we compare both methods using several standard parametrizations of the effective Lagrangian (see Table II). We recover what has already been pointed out in earlier references [15]. As a consequence of the large RTF surface energies, the RTF binding energies are somewhat lower than those obtained in RH, whereas the RTF surface densities with their remarkable long shoulder and a subsequent rapid falloff lead to surface thicknesses that are too large compared with the RH values.

In a series of investigations [15] the RTF method has been extended (RETF) by semiclassical $\hbar$ expansions as well as by the Wigner-Kirkwood approach. In these RETF calculations the surface thickness comes closer to the RH value, sometimes, however, even below it. The RETF energies, however, do not approximate the RH values appreciably better than the RTF values. Since for our purposes we have to calculate several thousands of nuclei we preferred the RTF method with its smaller numerical amount.

On the basis of the RTF equations (9)–(15) and the realistic NL1 parametrization we calculated nuclei in a large band around the line of β stability in the (N,Z) plane of the chart of nuclides. The results of these extensive ground-state calculations are plotted in Fig. 1. The solid contour lines connect nuclei with constant nucleon binding energy B/A. The open squares around the calculated stability line represent stable nuclei.

TABLE II. RMF parameter sets. Nucleon and meson masses are given in MeV. $C_i^2=g_i^2(M/m_i)^2, \quad i=s,v,\rho.$

	NL-Z [11]	NL1 [11]	NL-SH [17]
M (MeV)	938.90	938.00	939.00
m_s (MeV)	488.67	492.25	526.059
m_v (MeV)	780.00	795.36	783.00
m_ρ (MeV)	763.00	763.00	763.00
C_s^2	373.2479	373.1760	347.533
C_v^2	241.4392	245.4580	240.997
C_ρ^2	35.6700	37.4175	29.0954
b	0.0027922	0.0024578	0.0012747
c	-0.0039347	-0.0034334	-0.0013308

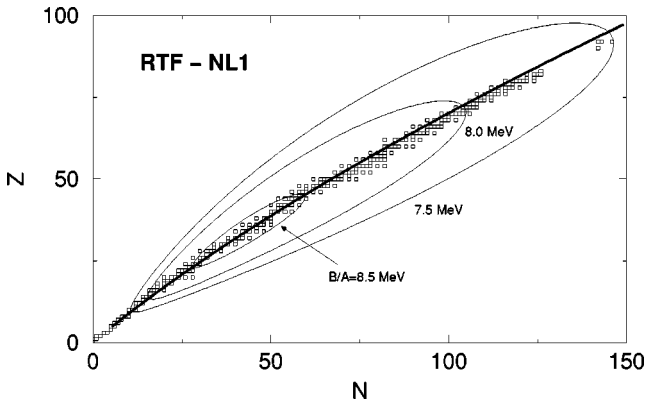

FIG. 1. Chart of nuclides with line of β stability and contour lines for some values of the binding energy per nucleon B/A extracted from RTF ground-state calculations using the parameter set NL1. The open squares represent stable nuclei.

B. Compressed nuclei

For uniform infinite symmetric nuclear matter (INM) phenomenological thermodynamics defines the (thermodynamic) pressure p_{th} at zero temperature by

$$p_{th}=\rho^2\frac{d}{d\rho}\left(\frac{\mathcal{E}(\rho)}{\rho}\right), \tag{17}$$

where ρ is the baryon density and $\mathcal{E}$ is the energy density depending on the baryon density. Also, in the case of a field-theoretical description of nuclear matter this expression—now with meson fields depending on source densities—defines the (thermodynamic) pressure for a uniform system.

Field theoretically, the energy density $\mathcal{E}$ of a system must be identified with the quantum-mechanical expectation value of the T_{00} component of the energy momentum tensor (see, e.g., [5]). For a homogeneous and isotropic fluid at rest the diagonal elements of the expectation value of the stress tensor are equal, and the nondiagonal elements vanish. Thus, a hydrodynamic scalar pressure p_{hydr} can be defined by

$$p_{hydr}\equiv\frac{1}{3}\sum_{i=1}^{3}\langle T_{ii}\rangle. \tag{18}$$

In the case of the RMF approximation the expectation value of the stress tensor can be specified, and for uniform systems the hydrodynamic pressure p_{hydr} turns out to be identical with the thermodynamic pressure p_{th} (see, e.g., [5]). One refers to thermodynamic consistency of the two pressure definitions in the RMF case for uniform systems.

As first steps to finite systems we have studied in Ref. [16] semi-infinite isospin-symmetric nuclear matter (SINM) as well as spherically symmetric nuclei treating them in the RTF approximation. Now, a *local* RTF energy-momentum tensor $T_{\mu\nu}$ and therefore a *local* hydrodynamic pressure p_{hydr} can be defined following a general procedure [16]. From the

local energy density $\mathcal{E}$ a *local* (thermodynamic) pressure $p_{\rm th}$ may be obtained by generalizing the definition (17),

$$p_{\rm th}=\rho^2\frac{\delta}{\delta\rho}\left(\frac{\mathcal{E}}{\rho}\right), \tag{19}$$

with the variational derivative denoted by δ. The two local RTF pressures are no more equal in the surface region, and we gave arguments [16] that the hydrodynamic definition of a local pressure via the stress tensor is the adequate one in order to describe compressional properties.

As the equivalent of external fields, that compress finite nuclei, constraints depending on the nuclear density were introduced in nonrelativistic approaches (see, e.g., Refs. [12]). Analogously one can add to the RMF energy density external constraints constructed in such a way that they reflect the specific external influence that leads to nuclear compression. Compression effects can be produced by external baryonic as well as mesonic effects. Thus, the external constraint could depend on the baryon field as well as on the meson fields, or even be of gravitational origin in astrophysical problems.

In a first approach we assume the constraint $\mathcal{C}$ to depend only on the total baryon density $\rho=\rho_{\rm n}+\rho_{\rm p}$. The constrained energy density $\mathcal{E}_{\rm CRTF}$ of the nucleus is, therefore,

$$\mathcal{E}_{\rm CRTF}=\mathcal{E}_{\rm RTF}(\chi,\chi',\rho_{\rm p},\rho_{\rm n})+\mathcal{C}(\rho). \tag{20}$$

χ denotes the set of the four fields ϕ_0, V_0, b_{00}, and A_0. χ' are their derivatives with respect to the radial distance r. In the bulk part, where thermodynamic and hydrodynamic pressure are equal, the external pressure $p_{\rm ext}$ is

$$p_{\rm ext}=\rho^2\frac{\partial}{\partial\rho}\left(\frac{\mathcal{C}(\rho)}{\rho}\right). \tag{21}$$

The variational principle, that the total energy including the constraint part be stationary,

$$\delta\left(4\pi\int_0^\infty[\mathcal{E}_{\rm RTF}(r)+\mathcal{C}(\rho)-\mu_{{\rm n}_\mathcal{C}}\rho_{\rm n}(r)-\mu_{{\rm p}_\mathcal{C}}\rho_{\rm p}(r)]r^2dr\right)=0, \tag{22}$$

then gives the CRTF equations for the constrained system:

$$\left(\frac{\partial\mathcal{C}(\rho)}{\partial\rho_{\rm p}}\right)+g_{\rm v}V_0(r)+g_\rho b_{00}(r)+eA_0(r)+\epsilon^\star_{\rm F_p}(r)=\mu_{{\rm p}_\mathcal{C}},\quad (r\leqslant\tilde{r}_{\rm u_p}), \tag{23}$$

$$\left(\frac{\partial\mathcal{C}(\rho)}{\partial\rho_{\rm n}}\right)+g_{\rm v}V_0(r)-g_\rho b_{00}(r)+\epsilon^\star_{\rm F_n}(r)=\mu_{{\rm n}_\mathcal{C}},\quad (r\leqslant\tilde{r}_{\rm u_n}), \tag{24}$$

where

$$\frac{\partial\mathcal{C}(\rho)}{\partial\rho_{\rm p}}=\frac{\partial\mathcal{C}(\rho)}{\partial\rho_{\rm n}}=\frac{d\mathcal{C}(\rho)}{d\rho}. \tag{25}$$

The explicit suffix $\mathcal{C}$ in the Lagrange multipliers $\mu_{{\rm n}_\mathcal{C}}$ and $\mu_{{\rm p}_\mathcal{C}}$ points to the fact that they will depend on the constraint and therefore be different from the ground-state case, Eqs. (13),(14). The CRTF equations for the fields do not differ explicitly from the unconstrained case, Eqs. (9)–(12), although via the coupling of all equations the resulting fields depend implicitly on the external pressure. The tilde in Eqs. (23),(24) indicates that the classical turning points also depend on the constraint.

In order to find an appropriate functional ansatz for the constraint, we are guided by the pocket model for compressed SINM which was introduced in Ref. [12]. For a simple, but realistic energy density it was found that with the class of polynomial constraints

$$\mathcal{C}_{q,\beta}(\rho(z))=\frac{K_\infty}{18}\frac{\rho^2(z)}{\rho_{\rm c}}\left[\frac{\rho(z)}{\rho_{\rm c}}(q^{-2\beta}-q^2)-2q^{-2\beta}+2q\right], \tag{26}$$

the compressed density can be obtained analytically as

$$\rho(z)=\frac{\rho_{\rm c}}{1+{\rm e}^{(z/\alpha_{\rm c})}}, \tag{27}$$

where

$$\alpha_{\rm c}=\alpha_0 q^\beta=\alpha_0\left(\frac{\rho_{\rm c}}{\rho_0}\right)^\beta. \tag{28}$$

α_0 is the ground-state value of the surface-diffuseness parameter. q is the ratio $\rho_{\rm c}/\rho_0$ of the SINM compressed bulk density $\rho_{\rm c}$ and the SINM saturation bulk density ρ_0. The parameter β controls how the variation of the bulk density is coupled to the variation of the surface density. It was found in Ref. [12] that the compression mode with $\beta=1$ leads to the minimum of the surface tension. The local pressure averaged over the surface region turned out to be smallest for this antiscaled mode. Thus, here the surface is, compared to other modes, relatively free, and tends to minimize the surface tension. The surface region cannot be totally without pressure since it is coupled to the compressed bulk part of SINM. The antiscaled mode $\beta=1$, although lowest in surface energy, is experimentally not distinguished from other modes. In heavy-ion collisions, e.g., the surface regions of the two colliding nuclei are not free, since compression just starts in this region. The monopole nuclear breathing mode microscopically [1] as well as in a hydrodynamical approach [13] is well described by a scaled density. This corresponding static mode with $\beta=-1/3$ was found in Ref. [12] to have a surface tension even larger than for the mode with $\beta=0$ that is described by multiplying the density with a constant factor.

In finite nuclei there are compression effects even in the ground-state case ($\mathcal{C}=0$) caused by the surface tension and the Coulomb interaction. The central value of the ground-state density $\rho^{\rm g.s.}(r)$, therefore, differs from the SINM saturation value ρ_0. Due to this effect the central compression

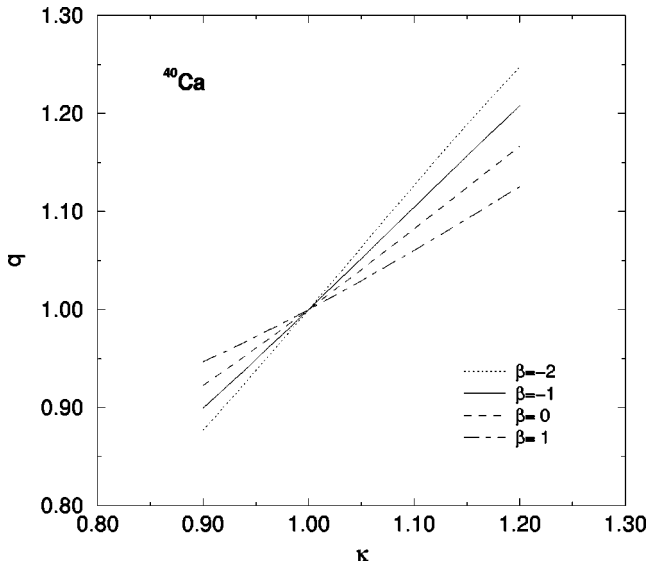

FIG. 2. The central compression ratio q as function of the compression parameter κ and the surface mode β. The results were obtained by CRTF compression calculations for the nucleus ^{40}Ca using the parameter set NL1.

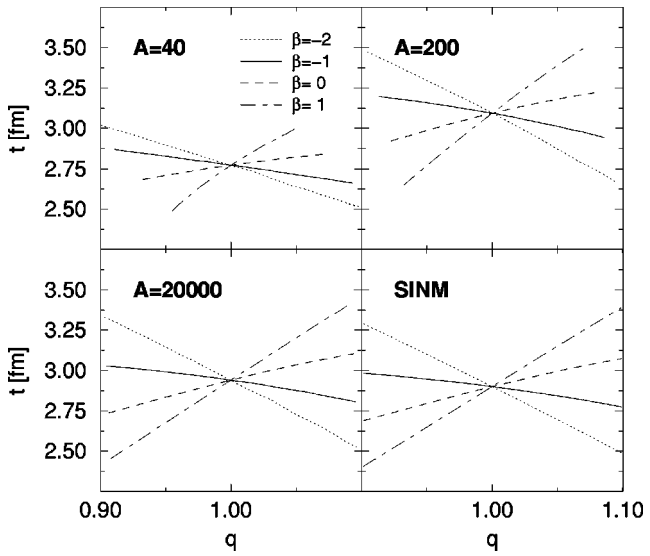

FIG. 3. 90–10 % surface thickness t as function of the central compression ratio q for some $N=Z$-nuclei with Coulomb interaction switched off. For comparison the results from symmetric SINM calculations are shown, too.

ratio cannot be fixed in advance in compression calculations for finite nuclei. Therefore, we adjust expression (26) in the following way:

$$\mathcal{C}^{\mathrm{RTF}}_{\kappa,\beta}(\rho(r))=\frac{K_\infty}{18}\frac{\rho^2(r)}{\rho(0)}\left[\frac{\rho(r)}{\rho(0)}(\kappa^{-2\beta}-\kappa^2)-2\kappa^{-2\beta}+2\kappa\right]. \tag{29}$$

The parameter κ now controls the magnitude of the central compression, with $\kappa=1$ corresponding to the ground state ($\mathcal{C}=0$). The parameter β specifies the surface compression.

For fixed values of κ and β the set of CRTF equations for compressed nuclei, i.e., Eqs. (9)–(12), (23),(24), and (29) must now be solved iteratively. In each iteration step the Lagrange multipliers $\mu_{\mathrm{p}_\mathcal{C}}$ and $\mu_{\mathrm{n}_\mathcal{C}}$ have to be adjusted in a such way that neutron and proton numbers are kept fixed. The resulting compression ratio in the nuclear bulk,

$$q=q(\kappa,\beta)\equiv\frac{\rho(0;\kappa,\beta)}{\rho^{\mathrm{g.s.}}(0)}, \tag{30}$$

can be determined after self-consistency has been reached.

The SINM limit of the set of CRTF equations is obtained by neglecting the curvature terms in Eqs. (9)–(11) and by replacing $\rho(0)$ by the SINM bulk density ρ_c in the constraint (29). Together with Eqs. (23),(24) these equations have to be solved for a given value of κ. The bulk density ρ_c is obtained from the balance between the nuclear bulk pressure and the external pressure p_{ext} given by Eq. (21).

In Fig. 2 the dependence of the central compression ratio q, Eq. (30), on the parameter κ is shown for several compression modes β for the nucleus ^{40}Ca. An approximate linear relation between q and κ can be seen for all values of β. q nearly equals κ in the case of $\beta=-1$.

The influence of the compression mode β on the surface region of finite nuclei is illustrated in Fig. 3. For several $N=Z$ nuclei with Coulomb interaction switched off, the 90–10 % surface thickness t is displayed as a function of the central compression ratio q. Experiments are expected to compress the bulk as well as the surface region. Thus, realistic constraints (29) seem to be those that lead to surface thicknesses t decreasing with increasing q.

A further possible approach to compressed nuclei is obtained from directly distorting the ground-state density. We make the following two-parametric ansatz for neutron and proton densities:

$$\rho_{\mathrm{n,p}}(r;q,\beta)=q\rho^{\mathrm{g.s.}}_{\mathrm{n,p}}\left(\frac{r}{q^\beta}\right). \tag{31}$$

The compression ratio q, assumed to be equal for neutron and proton densities, is given by

$$q=\frac{\rho_{\mathrm{n,p}}(0)}{\rho^{\mathrm{g.s.}}_{\mathrm{n,p}}(0)}. \tag{32}$$

Recalculating neutron and proton numbers,

$$N=4\pi\int_0^\infty\rho_{\mathrm{n}}(r;q,\beta)r^2dr=4\pi q^{(3\beta+1)}\int_0^\infty\rho^{\mathrm{g.s.}}_{\mathrm{n}}(r')r'^2dr', \tag{33}$$

$$Z=4\pi q^{(3\beta+1)}\int_0^\infty\rho^{\mathrm{g.s.}}_{\mathrm{p}}(r')r'^2dr', \tag{34}$$

one sees that they are only conserved in the scaling case $\beta=-1/3$. The compressed densities (31) are now set into the field equations (9)–(12) as source terms, and then the set of RTF equations can be solved in a straightforward way. The

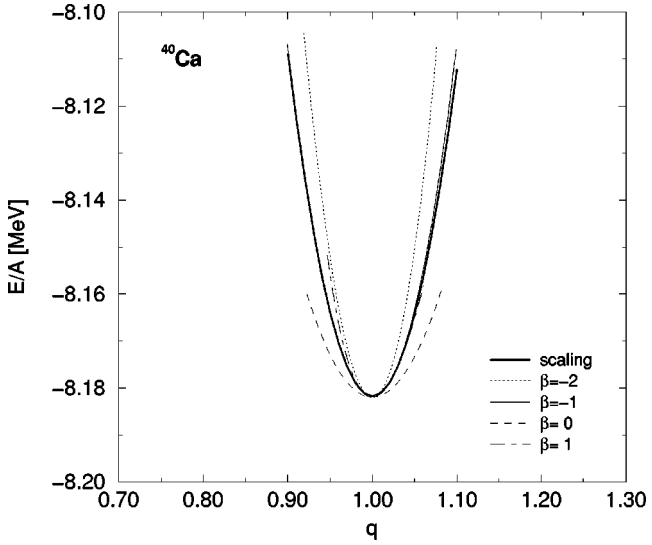

FIG. 4. Energy per particle of the nucleus ^{40}Ca as function of the central compression ratio q for several CRTF compression modes β. For comparison the scaling results (bold solid line) are shown, too.

proper CRTF equations (23),(24) could be used conversely to determine the constraint $\mathcal{C}$ that is responsible for the scaling of nuclear densities.

C. Energies of compressed nuclei

The intrinsic pure nuclear energy of a compressed nucleus follows by integration after inserting the compressed densities and respective mesonic and electromagnetic fields into the expression (7) for the energy density $\mathcal{E}_{\mathrm{RTF}}$. We have carried through calculations of many compressed nuclei on the basis of the external constraint (29) with its two parameters κ and β that allow us to compress the nuclear bulk accompanied by a special surface density change. As examples for our CRTF results we present Figs. 4 and 5 where the energies per nucleon are plotted for several surface

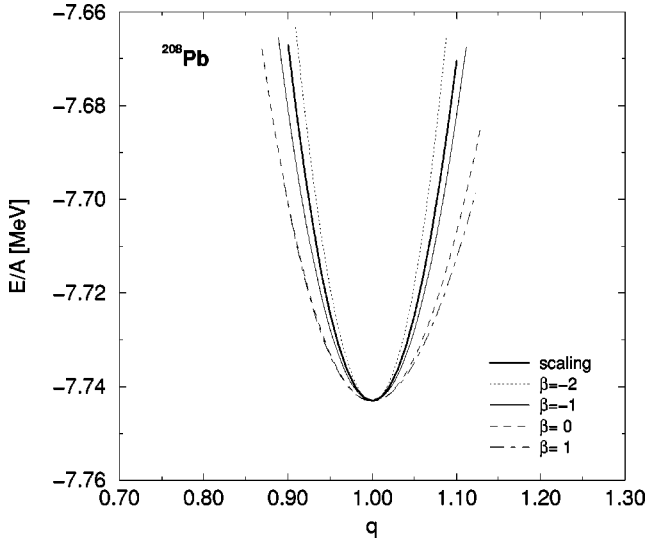

FIG. 5. Same as Fig. 4 for the nucleus ^{208}Pb.

modes β for the nuclei ^{40}Ca and ^{208}Pb. We used the NL1 parametrization of the effective Lagrangian. The energies per nucleon are plotted as function of the central compression ratio q [see Eq. (30)]. In addition also the energies for the case of scaled densities are given in both figures by solid continuous lines. They are reproduced quite well by the CRTF curves with parameter $\beta \approx -1$ in the constraint (29).

Due to the influence of Coulomb effects as well as due to compression from the surface tension, finite compressed nuclei do not show the clearly arranged behavior of the surface energy of SINM obtained in Ref. [12]. From Figs. 4 and 5 one can read off, e.g., that the compression mode lowest in energy is given by $\beta=0$ in the case of compressed ^{40}Ca, whereas for the large ^{208}Pb nucleus the $\beta=1$ mode is favored energetically. This lowest mode corresponds to the antiscaled mode in the pocket model of Ref. [12] which could be interpreted as the mode where the external constraint leaves the surface as free as possible.

For a study of the energy behavior under small compression one can expand the energy E/A per nucleon of a finite nucleus around the ground-state central density $\rho^{\mathrm{g.s.}}(0)$:

$$\left(\frac{E}{A}\right)(\rho_c)=\left(\frac{E}{A}\right)[\rho^{\mathrm{g.s.}}(0)]+\frac{1}{18}K_A\left(\frac{\rho_c-\rho^{\mathrm{g.s.}}(0)}{\rho^{\mathrm{g.s.}}(0)}\right)^2+\cdots. \tag{35}$$

The finite nucleus incompressibility

$$K_A\equiv 9\left[\rho_c^2\frac{\partial^2(E/A)}{\partial\rho_c^2}\right]_{\rho_c=\rho^{\mathrm{g.s.}}(0)} \tag{36}$$

can be extracted numerically from the energy calculations. It obviously depends on the compression mode given by the parameter β. From expression (35) those modes are seen to be energetically favored that also minimize the incompressibility K_A. The values of K_A obtained for model $N=Z$ nuclei with the Coulomb interaction switched off are shown in Fig. 6. One recovers from Fig. 6 the complicated energy behavior of compressed nuclei as a function of the mass number A and the compression mode which was found also from Figs. 4 and 5. The case $\beta=-2$ (open circles) with K_A larger than the INM value K_∞ (solid square on the vertical axis of Fig. 6) is traced back to a surface tension which increases with compression. This unexpected behavior also showed up in the pocket model for SINM matter of Ref. [12]. For comparison the scaling case is also shown in Fig. 6. One sees in particular how well the K_A values in the limit of large mass numbers A approach the K_∞ value for the NL1 Lagrangian calculated independently.

D. Stability properties of compressed nuclei

One can now compare the energies of a series of compressed nuclei following from a given external constraint (29), and from there obtain information on their stability properties under the respective compression. Instability shows up by a final configuration—following, e.g., after β decay or particle evaporation or also after fission—that is

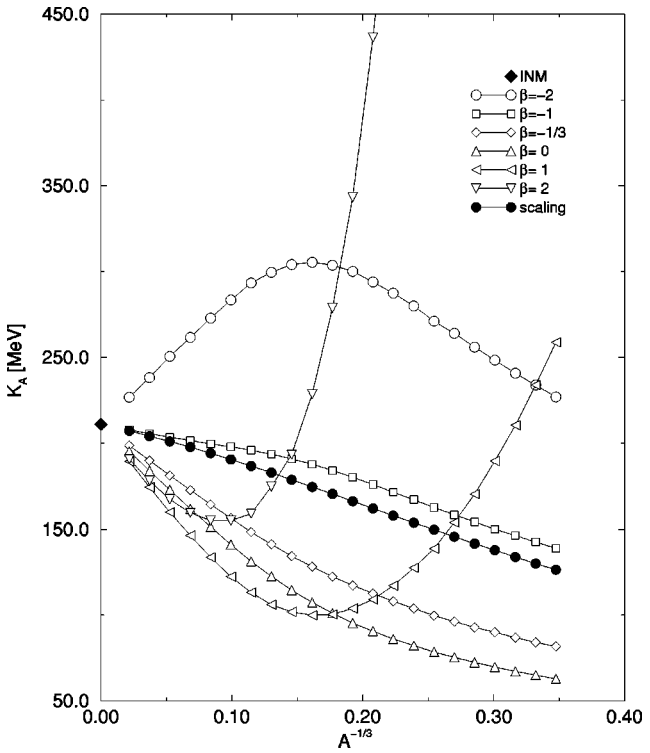

FIG. 6. Finite nucleus incompressibility K_A for $N=Z$ nuclei, with Coulomb interaction switched off, as a function of $A^{-1/3}$ for several surface compression modes β. The symbol on the vertical axis represents the INM value K_∞.

lower in energy under the same external constraint. With this assumption the line of β stability as well as the proton and neutron drip lines are defined in a way analogous to the standard case of uncompressed nuclei in vacuo. Thus, the line of β stability for nuclei compressed according to the ratio q, Eq. (30), is given by

$$\left.\frac{\partial B(A,I;q,\beta)}{\partial I}\right|_{A;q,\beta}=0, \tag{37}$$

where I denotes the relative neutron excess

$$I\equiv\frac{N-Z}{N+Z}. \tag{38}$$

Also the drip lines are obtained from the elementary formulas well known from textbooks (see, e.g., [18]). We have extracted the stability lines for several compression ratios q from the energies calculated for scaled densities where the full self-consistency problem of the CRTF equations (23) and (24) can be avoided. In Fig. 7 we display the stability lines calculated for q parameters ranging from 1 up to 2. The lines are shifted in the (N,Z) plane towards nuclei with increasing neutron excess. Therefore, nuclei are predicted to become β^+ unstable under compression. The decay of a proton into a neutron obviously leads to a configuration more stable by lowering the Coulomb energy of the original compressed nucleus. The subsequent increase of energy by the effect of the neutron-proton asymmetry clearly helps to stop these decays.

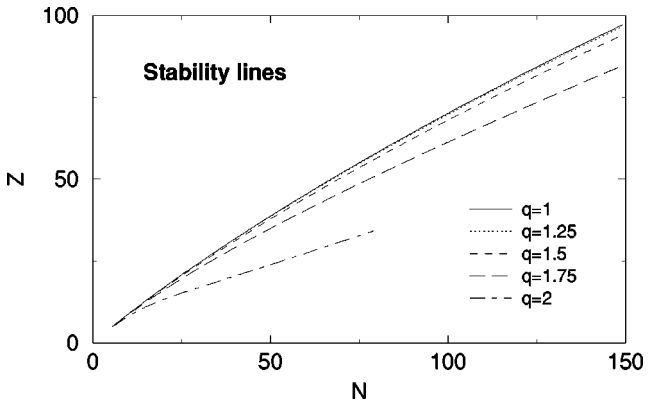

FIG. 7. Lines of β stability of compressed nuclei for several values of the central compression ratio q. The stability lines were extracted from RTF scaling calculations for the parameter set NL1.

The proton drip line as upper boundary and the stability line as lower boundary of a shadowed area in the (N,Z) plane are displayed in Fig. 8 for several compression ratios q up to $q=2$. It can be deduced from this figure that nuclei, originally stable under vanishing pressure, are getting into β^+ instability regions after compression, and eventually after a critical compression they become proton unstable emitting a proton in order to reduce the Coulomb repulsive energy. In contrast to the proton drip lines the neutron drip lines were found to be shifted less under nuclear compression, and into the opposite direction.

E. Fission of compressed nuclei

In the picture based on the liquid drop model and on mass formulas the height of the potential energy barrier for the fission process depends on the interplay between nuclear surface energy and Coulomb energy. Both are influenced by compression. Thus, also the fission process must depend on compression. The ratio of the changes of the Coulomb and the surface energy for a quadrupole deformation defines the fissility parameter

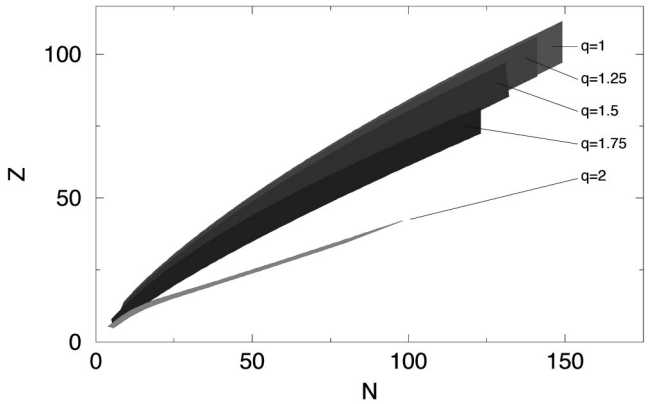

FIG. 8. Regions between the proton drip line (upper boundary) and line of β stability (lower boundary) of compressed nuclei for several values of the central compression ratio q.

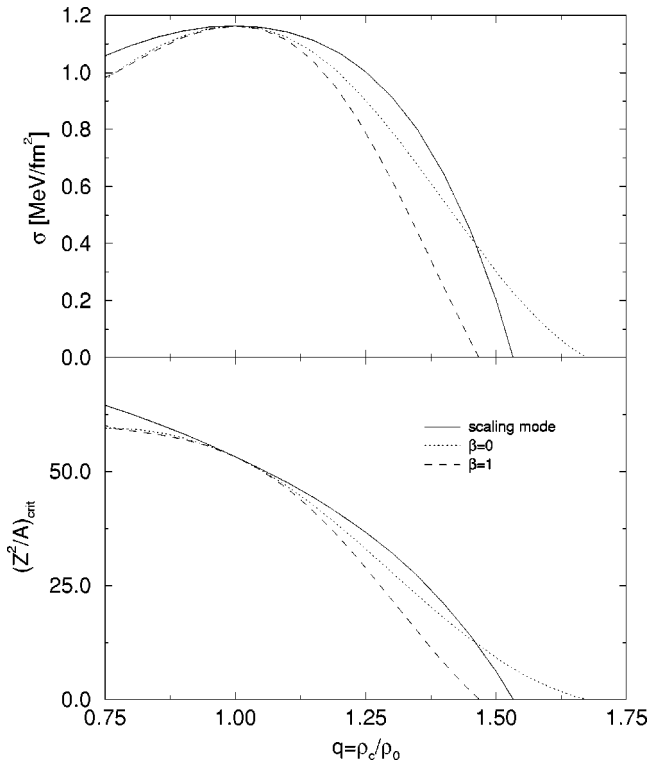

FIG. 9. The critical value $(Z^2/A)_{\mathrm{crit}}$ and the surface tension σ as functions of the compression ratio q obtained from SINM scaling as well as CRTF calculations using the parameter set NL1.

$$x=\frac{Z^2/A}{(Z^2/A)_{\mathrm{crit}}}, \quad (Z^2/A)_{\mathrm{crit}}\equiv\frac{40\pi\sigma r_c^3}{3e^2}, \tag{39}$$

where r_c is the nuclear radius parameter following from the bulk nuclear density, and σ is the nuclear surface tension. For a critical value of Z^2/A corresponding to $x=1$ the spherical shape becomes unstable with respect to quadrupole deformations, indicating the onset of spontaneous fission. For nuclei in vacuo this critical value is around $(Z^2/A)_{\mathrm{crit}}=50$.

Now, if nuclei are compressed the parameter r_c as well as σ in expression (39) change. The change of σ does not only depend on the bulk compression ratio q but also on the surface compression mode. The dependence of the surface tension on the compression has been calculated in Refs. [12] using nonrelativistic descriptions of the plane surface in SINM. The CRTF results resemble qualitatively the nonrelativistic case. In particular the stationarity of the surface tension at saturation density, irrespective of the surface mode, is reproduced corroborating again a theorem found by Myers and Swiatecki in Ref. [19]. In the following quantitative investigations we use the results obtained for σ in the scaling mode and also for the CRTF modes $\beta=0$ and $\beta=1$ (see upper part of Fig. 9). For these modes the surface tension is maximum at saturation density, and is therefore reduced with increasing compression. With these results on σ we evaluate $(Z^2/A)_{\mathrm{crit}}$ Eq. (39). In Fig. 9 (lower part) we have plotted the critical ratio $(Z^2/A)_{\mathrm{crit}}$ as a function of the compression ratio q. The vanishing of the surface tension is reflected in a vanishing of this ratio at about $q=1.6$. One concludes from the behavior of $(Z^2/A)_{\mathrm{crit}}$ that compression makes the nucleus unstable with respect to fission. The stabilizing surface tension is reduced and the destabilizing Coulomb energy is increased. Both effects reduce the fission barrier with increasing compression which at first sight might seem to be somewhat of a paradox.

III. OUTLOOK

We have introduced into the standard RTF procedure a constraint that is able to describe an external pressure exerted on nuclei. From the calculated energies of compressed nuclei conclusions were drawn about the stability properties of nuclei under pressure.

Nuclear shell effects cannot be taken into account by this CRTF approach. Therefore, it is a challenge to use the RH method with constraint in order to study shell effects in nuclei under compression. In particular the change of magic numbers is of interest. One could get, e.g., some insight whether special exotic nuclei—becoming magic under compression—might be produced in a reaction.

Further questions related to compressed nuclei that require, however, approaches with more subnucleonic degrees of freedom concern the onset of mesonic and even quark-gluonic condensation.

ACKNOWLEDGMENTS

We would like to thank P.-G. Reinhard for supplying us with his relativistic Hartree code and S. Typel for useful discussions.

[1] J. P. Blaizot, J. F. Berger, J. Dechargé, and M. Girod, Nucl. Phys. **A591**, 435 (1995).
[2] D. H. Youngblood, H. L. Clark, and Y.-W. Lui, Phys. Rev. Lett. **82**, 691 (1999).
[3] Z. Patyk, A. Baran, J. F. Berger, J. Dechargé, J. Dobaczewski, P. Ring, and A. Sobiczewski, Phys. Rev. C **59**, 704 (1999).
[4] Y. Aboussir, J. M. Pearson, A. K. Dutta, and F. Tondeur, At. Data Nucl. Data Tables **61**, 127 (1995).
[5] B. D. Serot and J. D. Walecka, Adv. Nucl. Phys. **16**, 1 (1986); P.-G. Reinhard, Rep. Prog. Phys. **52**, 439 (1989); Y. K. Gambhir, P. Ring, and A. Thimet, Ann. Phys. (N.Y.) **198**, 132 (1990); B. D. Serot and J. D. Walecka, Int. J. Mod. Phys. E **6**, 515 (1997).
[6] P. Möller, J. R. Nix, W. D. Myers, and W. J. Swiatecki, At. Data Nucl. Data Tables **59**, 185 (1995); W. D. Myers and W. J. Swiatecki, Nucl. Phys. **A601**, 141 (1996).
[7] W. D. Myers and W. J. Swiatecki, Phys. Rev. C **57**, 3020 (1998).
[8] W. Stocker and T. v. Chossy, Phys. Rev. C **58**, 2777 (1998).
[9] M. Arnould and K. Takahashi, Rep. Prog. Phys. **62**, 395

(1999).
[10] G. F. Bertsch and S. Das Gupta, Phys. Rep. **160**, 190 (1988); J. Aichelin, *ibid.* **202**, 233 (1991); T. Gaitanos, C. Fuchs, and H. H. Wolter, Nucl. Phys. **A650**, 97 (1999).
[11] P.-G. Reinhard, M. Rufa, J. Mahrun, and W. Greiner, Phys. Rev. Lett. **57**, 2916 (1986).
[12] M. Farine, J. Côté, J. M. Pearson, and W. Stocker, Z. Phys. A **309**, 151 (1982); M. Brack and W. Stocker, Nucl. Phys. **A388**, 230 (1982).
[13] M. Brack and W. Stocker, Nucl. Phys. **A406**, 413 (1983).
[14] B. D. Serot and J. D. Walecka, Phys. Lett. **87B**, 172 (1979).
[15] M. K. Weigel, S. Haddad, and F. Weber, J. Phys. G **17**, 619 (1991); M. Centelles, X. Viñas, M. Barranco, S. Marcos, and R. J. Lombard, Nucl. Phys. **A537**, 486 (1992); M. Centelles, X. Viñas, M. Barranco, and P. Schuck, Ann. Phys. (N.Y.) **221**, 165 (1993); C. Speicher, E. Engel, and R. M. Dreizler, Nucl. Phys. **A562**, 569 (1993); D. Von-Eiff, S. Haddad, and M. K. Weigel, Phys. Rev. C **50**, 1244 (1994).
[16] T. v. Chossy and W. Stocker, Phys. Rev. C **54**, 731 (1996).
[17] M. M. Sharma, M. A. Nagarajan, and P. Ring, Phys. Lett. B **312**, 377 (1993).
[18] J. M. Pearson, *Nuclear Physics: Energy and Matter* (Hilger, Bristol, 1986).
[19] W. D. Myers and W. J. Swiatecki, Ann. Phys. (N.Y.) **55**, 395 (1969).